Renewable Energy 252 (2025) 123347

Contents lists available at ScienceDirect

Renewable Energy

journal homepage: www.elsevier.com/locate/renene

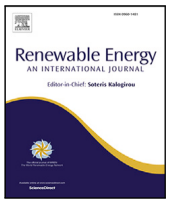

# Modeling moisture ingress in PV modules with different encapsulant and backsheet materials

Youri Blom [a,*], Daniel Jimenez Pelarda [a], Tabitha Minett [a], Ismail Kaaya [b,c,d], Nikoleta Kyranaki [b,c,d], Rudi Santbergen [a], Olindo Isabella [a], Malte Ruben Vogt [a,*]

[a] Delft University of Technology, Mekelweg 4, Delft, 2628CD, The Netherlands
[b] Imec imo-imomec, Thor Park 8320, Genk, 3600, Belgium
[c] Hasselt University imo-imomec, Martelarenlaan 42, Hasselt, 3600, Belgium
[d] EnergyVille imo-imomec, Thor Park 8320, Genk, 3600, Belgium

ARTICLE INFO

*Keywords:*
Moisture ingress
FEM simulation
Degradation
Analytical model

ABSTRACT

Increasing the operating lifetime of photovoltaic (PV) modules is a key factor in further reducing their levelized cost of electricity. Analytical degradation models typically use the external relative humidity (RH) as a stress factor, rather than the moisture concentration inside the module. This study presents a Finite Element Method (FEM) model, built in COMSOL Multiphysics, to simulate the moisture ingress inside a PV module. We explore the effects of different encapsulant and backsheet materials, as well as various climatic conditions, on moisture penetration. Overall, the impact of the climate has a larger impact on the moisture ingress than the choice of material, implying that the PV module design should be adjusted for different climates. As FEM simulations are computationally intensive, we also present an analytical model, based on empirically determined characteristics, to simulate the moisture ingress. This reconstruction can be done with a deviation lower than 0.05 for all conditions. Finally, our findings indicate that the relative moisture content (RMC) within the module serves as a more accurate stress factor than outdoor RH. Degradation rates over time found in literature are captured more accurately when deploying RMC.

## 1. Introduction

The levelized cost of electricity for photovoltaic (PV) modules has dramatically decreased by 89% from 0.445 USD/kWh in 2010 to 0.049 USD/kWh in 2022 [1]. A crucial factor in further reducing these costs is enhancing the reliability and operating lifetime of PV modules [2]. The lifespan of PV modules is significantly affected by various stress factors that degrade the performance over time [3]. To optimize energy production over the module's lifetime, understanding how stress factors cause degradation is essential.

Research literature has introduced several analytical models that describe the impact of stress factors on PV module degradation [4,5]. These models typically relate temperature (T), ultraviolet (UV) irradiation, and relative humidity (RH) to performance loss. However, it is important to note that degradation is not directly caused by RH but rather by the moisture within the PV module. Hassan et al. made a review on different failure mechanisms in solar panels, and explained that delamination and corrosion is triggered by chemical reactions with water in the encapsulant [6]. Similarly, Segbefia et al. made a review on moisture ingress in PV modules and argued that moisture ingress is the core of most degradation mechanisms and discuss the different techniques for measuring the moisture concentration inside the PV module [7]. In other work, Segbefia et al. demonstrated the effect of moisture ingress on a field-aged PV module, showing that the effect around the solar joints dominates [8]. Lastly, Koehl et al. propose a design for appropriate damp-heat tests and discuss how the design of the PV module affects the mass transport of water [9]. These studies indicates that lifetime prediction models can be improved by predicting the moisture content in PV modules.

Several studies have modeled moisture ingress using either Finite-Element-Method (FEM) models or analytical models to simulate different climatic conditions. Kempe et al. model the moisture ingress using finite-element analysis for different locations [10]. Similarly, Hulsmann et al. have simulated the water uptake of PV modules for different materials and climatic conditions [11]. Mitterhofer et al. used a FEM model to simulate the moisture ingress for more than 17,000 locations, and train a machine-learning algorithm to find correlations between climatic parameters and simulation results [12]. In different work, Mitterhofer et al. validate their FEM model with simulations

* Corresponding authors.
*E-mail addresses:* Y.Blom@tudelft.nl (Y. Blom), M.R.Vogt@tudelft.nl (M.R. Vogt).

https://doi.org/10.1016/j.renene.2025.123347
Received 3 October 2024; Received in revised form 25 April 2025; Accepted 2 May 2025
Available online 17 May 2025
0960-1481/© 2025 The Authors. Published by Elsevier Ltd. This is an open access article under the CC BY license (http://creativecommons.org/licenses/by/4.0/).

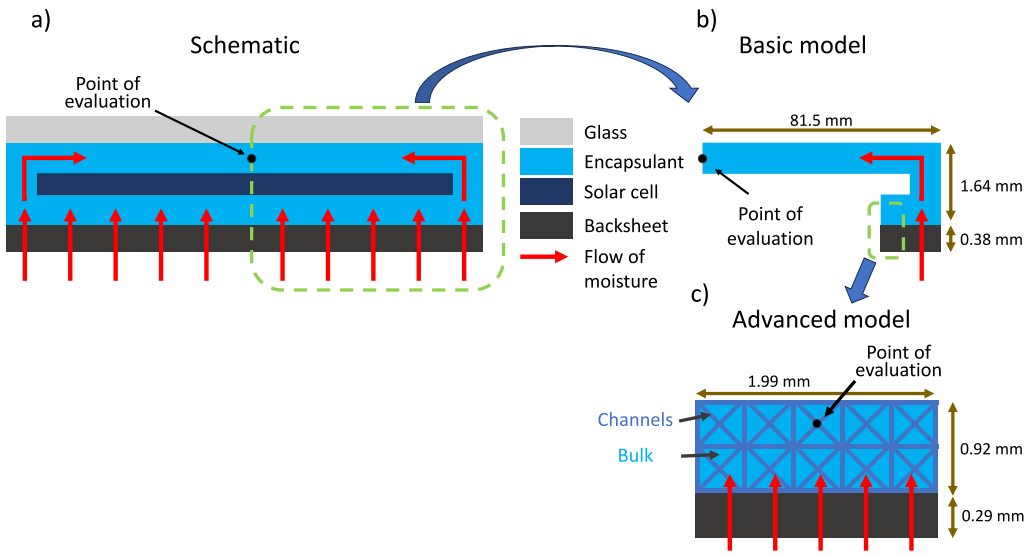


**Fig. 1.** (a) An overview of the considered schematic for the FEM model and (b) the translation into the developed model. The green dashed line indicates which part of the schematic is used in the basic model. The glass and solar cell have been removed as these materials are considered to be impermeable. Also, a part of the backsheet and encapsulant below the cell has been removed to reduce the computational effort. (c) The advanced model only considers a segment of the basic model (indicated with the green dashed line), as it is computationally intensive. For this model, the dual-transport model is implemented as proposed by Mitterhofer et al. [17].

in various climates [13]. In contrast to a FEM model, Coyle et al. developed an analytical model to express the relative concentration of water in CIGS solar cells [14]. Similarly, Marwaha et al. demonstrated an analytical model to quantify amount of moisture ingress in PV modules with a breathable backsheet [15]. These models often report the absolute water concentration, whereas the relative concentration to the saturation point is a more relevant metric for assessing degradation in PV modules [14].

This study presents a FEM model to simulate moisture ingress in crystalline silicon PV modules over their lifetime. We report relative moisture content ($RMC$) instead of the actual concentration. The simulations are conducted for various geographical locations to assess environmental impacts, and different encapsulant and backsheet materials to examine material choices. Given the computational intensity of FEM simulations, we also develop an analytical model based on empirical parameters derived from the FEM simulations. This model allows for predicting moisture ingress without needing further FEM simulations. Finally, we simulate power loss due to moisture-induced degradation across different climates and module materials using RMC as the stress factor instead of RH.

## 2. Methodology

This section outlines the implementation of the (FEM) model using COMSOL Multiphysics software [16]. We develop two versions of the model: a basic and an advanced model, as illustrated in Fig. 1. After describing each model, we compare their results with results from literature in two distinct methods.

### 2.1. Basic model

Both models are based on a two-dimensional representation, including a backsheet, encapsulant, solar cell, and glass, as illustrated on the left side of Fig. 1. Due to symmetry, the computational burden can be reduced by modeling only half of the cell. Since the solar cell and glass are considered impermeable [9,10], they are excluded from the simulation domain.

Although the model can output the concentration of every point in the encapsulant and backsheet, only the concentration above the cell is evaluated as corrosion mostly occurs at the ribbons at the front of the cell [18,19]. Consequently, we can exclude a portion of the encapsulant and backsheet below the cell from the simulation, as their moisture levels do not impact the concentration at the critical evaluation point. The exact values for all dimensions are reported in Appendix A. The overall structure of our model is comparable to the one developed by Mitterhofer et al. [12].

To simulate moisture ingress in the PV module, we consider water molecule diffusion through the backsheet and encapsulant, and we apply boundary conditions at the module's interface with the air. This diffusion is governed by Fick's second law of diffusion [20], written as

$$\frac{\partial C}{\partial t} = D \cdot \nabla^2 C, \tag{1}$$

where $C$ is the concentration, $t$ is the time, and $D$ is the diffusion coefficient of the material.

The diffusion coefficient depends on the module temperature ($T_{mod}$) and follows an Arrhenius relationship [7,21]

$$D = D_0 \cdot e^{-\frac{E_{a,D}}{R \cdot T_{mod}}}, \tag{2}$$

where $D_0$ is the diffusion pre-exponential constant, $E_{a,D}$ is the diffusion activation energy, and $R$ is the universal gas constant. $T_{mod}$ is the module temperature as determined with the Faiman model [22].

In addition to the diffusion coefficient, solubility coefficients ($S$) are crucial for describing moisture ingress. Solubility reflects the amount of water a material can absorb and is also modeled using an Arrhenius relationship

$$S = S_0 \cdot e^{-\frac{E_{a,S}}{R \cdot T_{mod}}}, \tag{3}$$

where $S_0$ is the solubility pre-exponential constant, and $E_{a,S}$ is the solubility activation energy.

At the interface between the backsheet and air, concentration can be determined using Henry's law [23], which states that the absorbed moisture in a polymer is proportional to the environmental RH [24]. It must be noted that this is a simplification which is more valid for ideal polymers, however we do not have experimental data which indicate a more suitable model.

$$\frac{C_{BS}}{S_{BS}} = p_{sat} \cdot RH_{eff}, \tag{4}$$

where $C_{BS}$ and $S_{BS}$ are the concentration and solubility of backsheet, respectively, $p_{sat}$ is the saturation pressure (modeled with the Antoine equation [25,26]), and $RH_{eff}$ is the effective relative humidity. $RH_{eff}$ differs from RH because the module temperature is different from the ambient temperature and can be calculated using the Magnus equation [11,27,28].

Similarly, the concentration at the encapsulant-backsheet interface is given by

$$\frac{C_{BS}}{S_{BS}} = \frac{C_{enc}}{S_{enc}}, \tag{5}$$

where $C_{enc}$ and $S_{enc}$ are the concentration and solubility of encapsulant. Eq. (5) is based on the assumption that Henry's law also applies to this interface [14].

To quantify the amount of moisture ingress, we evaluate $RMC$ at the point in the middle of the cell (indicated in Fig. 1). As described by Kyranaki [24], the $RMC$ is calculated with

$$RMC = \frac{C_{enc}}{S_{enc}} \tag{6}$$

Since both $C$ and $S$ are expressed in [$\mathrm{kg\,m^{-3}}$], $RMC$ is a unitless quantity.

### 2.2. Advanced model

The basic model assumes homogeneous Fickian diffusion across materials. However, literature suggests this may not accurately represent the behavior of polymeric materials used in encapsulants and backsheets [17,29]. Mitterhofer et al. [17] propose a more realistic approach by considering two distinct transport mechanisms: diffusion in bulk and channels. To simulate this, the encapsulant is split into two regions, namely the bulk and channels, as indicated in Fig. 1(c). The channels have a higher diffusion coefficient than the bulk, simulating the flow in nanochannels [30], which can be written as

$$D_b = \alpha \cdot D_c, \tag{7}$$

where $D_b$ and $D_c$ are the bulk and channel diffusion coefficients, respectively, and $\alpha$ describes the ratio between both coefficient assumed to be $3.1 \times 10^{-6}$ as derived by Mitterhofer et al. [17]. A more detailed description on the implementation on the advanced model in COMSOL is provided in Appendix B.

### 2.3. Validation

We perform two types of validations for our model. For the first comparison, we compare our models' results with measurements and simulations conducted by Kyranaki et al. [24], as depicted in Fig. 2. The test sample lacks a solar cell, so our model geometry is adjusted accordingly. These experiments are performed in a climate chamber with a controlled temperature and relative humidity of 50 °C and 80%, respectively. Kyranaki's simulation assumes Fickian diffusion, aligning well with our basic model's results. In contrast, the advanced model using the dual channel approach accurately matches the measured moisture ingress, suggesting our basic model behaves similarly to Kyranaki's, and any deviations in measurements are due to the assumption of Fickian diffusion.

Fig. 3 illustrates a comparison between our basic model's simulation and the model by Mitterhofer et al. [12]. Both simulations evaluate moisture concentration in a PV module in Manaus, Brazil, over 10 years. Given that literature models assume Fickian diffusion, we use our basic model for comparison. The similarity in results indicates that our model can also be used for simulating moisture ingress under outdoor conditions.

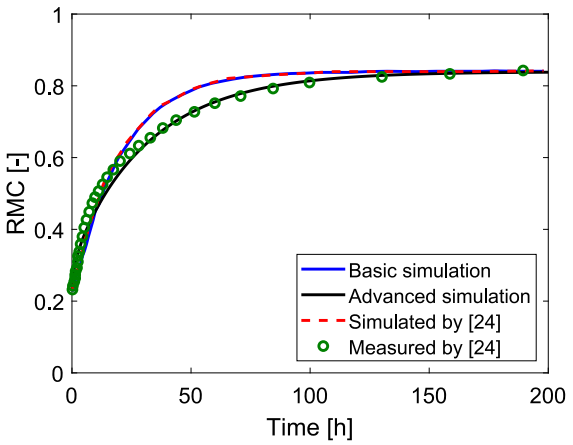


**Fig. 2.** A comparison of the $RMC$ inside the test sample consisting of backsheet and encapsulation (without solar cell) in a climate chamber predicted by our models and simulated and measured by Kyranaki et al. [24]. The advanced non-Fickan model shows better agreement with the experimental data compared to the basic Fickian models.

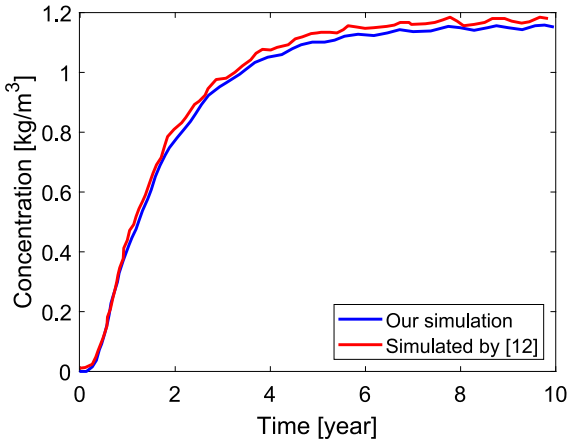


**Fig. 3.** A comparison of the water concentration inside a PV module under real world conditions (Manaus in Brazil) predicted by our model and simulated by Mitterhofer et al. [12].

### 2.4. Choice of model

While the advanced model demonstrates higher accuracy in climate chamber experiments, it demands significantly more computational time. For instance, simulating the experiment for 200 h (about 8 days) of exposure time with the basic model takes 18 s, whereas the advanced model requires 29 min. Considering the impracticality of simulating 20 years of outdoor conditions with the advanced model, we chose to use the basic model for the remainder of this work.

This choice is justified because non-Fickian behavior is more pronounced at higher RH values [31] and elevated cell temperatures [32]. Since both temperature and RH are higher in experimental tests compared to outdoor conditions, the error from assuming Fickian diffusion is expected to be smaller in real-world scenarios. However, it should be realized that although this is the case for ground-mounted PV systems, building integrated PV (BIPV) systems can experience temperatures in the range of 60-80 °C [33]. Therefore, the error from assuming Fickian diffusion can be larger when our model is applied to BIPV systems.

## 3. Case study

We simulate The moisture ingress for PV modules with different encapsulant and backsheet materials in various climates. As encapsulant, we have selected ethylene-vinyl acetate (EVA), thermoplastic

**Table 1**
The parameters of the different materials. The first three materials are encapsulants obtained from [34]. The latter four materials are used as backsheet and the values are obtained from [35].

| | $D_0$ | $E_{a,D}$ | $S_0$ | $E_{a,S}$ |
|---|---|---|---|---|
| | [$m^2$ $s^{-1}$] | [kJ $mol^{-1}$] | [g $m^{-3}$] | [kJ $mol^{-1}$] |
| EVA | $2.32 \times 10^{-4}$ | 38.1 | $1.81 \times 10^{6}$ | 16.7 |
| TPO | $5.22 \times 10^{-2}$ | 52.9 | $1.56 \times 10^{6}$ | 24.6 |
| PDMS | $3.43 \times 10^{-5}$ | 26.8 | $8.05 \times 10^{4}$ | 11.2 |
| PET | $6.02 \times 10^{-6}$ | 39.2 | $7.08 \times 10^{9}$ | 43.2 |
| TPT | $5.97 \times 10^{-7}$ | 33.1 | $3.03 \times 10^{10}$ | 44.8 |
| $TPSiO_x$ | $1.01 \times 10^{-9}$ | 17.2 | $1.01 \times 10^{14}$ | 70.0 |
| PA | $2.27 \times 10^{-3}$ | 53.9 | $2.98 \times 10^{9}$ | 41.6 |

**Table 2**
The effective RH, average module temperature, and change in module temperature of each location. The change in module temperature represents the seasonal fluctuation of the module temperature.

| | effective RH [-] | Average $T_{mod}$ [°C] | $\Delta T_{mod}$ [°C] |
|---|---|---|---|
| Manaus | 0.59 | 33 | 4.4 |
| Jakarta | 0.56 | 33 | 6.6 |
| Los Angeles | 0.51 | 22 | 12 |
| Freiburg | 0.57 | 14 | 25 |
| Dubai | 0.40 | 33 | 18 |
| Almeria | 0.50 | 23 | 18 |
| Portland | 0.64 | 11 | 26 |
| Oslo | 0.61 | 9.4 | 28.2 |

polyolefin (TPO) and Polydimethylsiloxane (PDMS) used as material. For the backsheet, polyethylene terephthalate (PET), Tedlar-PET-Tedlar (TPT), Tedlar-PET-$SiO_x$ ($TPSiO_x$), and Polyamide (PA) are used. The properties of all the encapsulants and backsheets are obtained from Kempe et al. [34] and Hülsmann et al. [35], respectively. Each material's properties are characterized by parameters shown in Table 1, which are used in the simulations.

We also analyzed how different climatic conditions affect moisture ingress. Simulations were conducted for eight geographical locations representing various climate zones according to the Köppen-Geiger (KG) classification [36]. The hourly climate data for all locations are obtained from Meteonorm version 7.2 [37].

The selected climates were:

- Tropical, which is represented by Manaus (Brazil) and Jakarta (Indonesia).
- Temperate, which is represented by Los Angeles (United States) and Freiburg (Germany).
- Arid, which is represented by Dubai (United Arab Emirates) and Almeria (Spain).
- Continental, which is represented by Portland (United States) and Oslo (Norway).

Each location can be characterized by different stress factors, summarized in Table 2, which are all factors relevant to the moisture ingress. This includes the average effective RH, which is also used in Eq. (4), the average module temperature, and the seasonal deviation in temperature. The latter stress factor is explained more in Appendix C.

## 4. Results

To assess the impact of different materials and climates on the moisture ingress in PV modules, we simulate these conditions over a period of 20 years. We examine how variations in the materials used for encapsulant and backsheet, as well as different geographical locations, influence the moisture behavior in the modules.

### 4.1. Effect of materials

First, we analyze the impact of the material choice on the moisture ingress. As example, we show the simulations under operating conditions typical for Freiburg, Germany. Fig. 4 illustrates the simulated moisture ingress for each material.

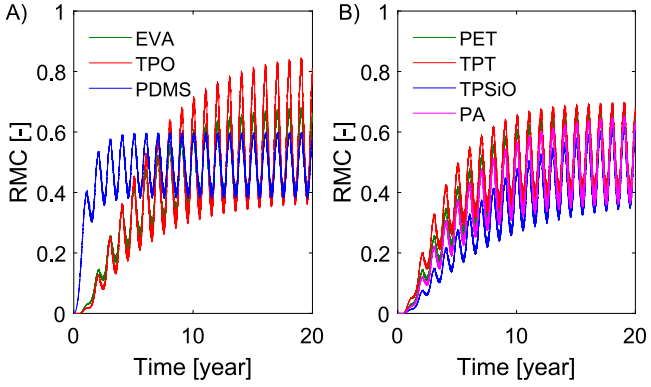


**Fig. 4.** The moisture ingress for different encapsulants (A) and backsheets (B). The reference scenario is a PV module with EVA and PET as encapsulant and backsheet, simulated in Freiburg.

To facilitate a more quantitative comparison, we define and evaluate several characteristics for each simulation:

- The equilibrium relative moisture content ($RMC_{eq}$), which is defined as the average $RMC$ value in the last year.
- The saturation time ($\tau_{95\%}$), which is defined as the time it takes for $RMC$ to reach 95% of $RMC_{eq}$.
- The seasonal deviation ($A$), which is defined as the largest difference in $RMC$ within one year.
- The ingress time ($\tau_{0.01}$), which is defined as the time it takes before the $RMC$ reaches a value of 0.01.

Fig. 5 shows these characteristics for each situation. For all materials the $RMC_{eq}$ is relatively similar for all simulations ranging from 0.48-0.59. This is because this value is mostly dependent on the climatic conditions, which will be discussed further at the end of this section.

The choice of encapsulants significantly affects the moisture ingress rate. PDMS, due to its low activation energy for diffusion, has a higher diffusion coefficient, resulting in faster moisture ingress and lower values for $\tau_{95\%}$ and $\tau_{0.01}$. This suggests quicker moisture related degradation for modules encapsulated with PDMS.

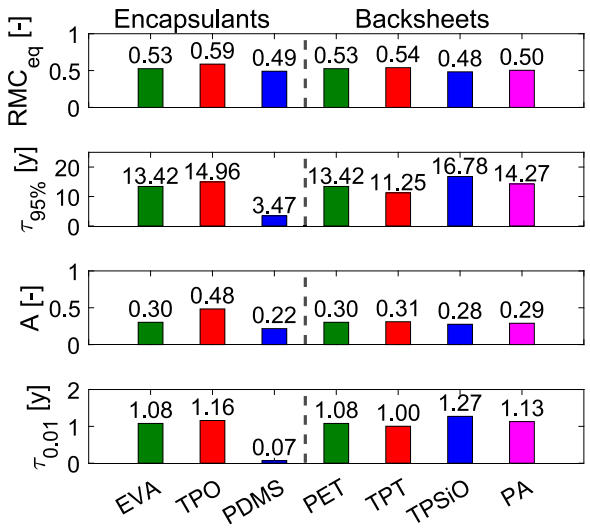


**Fig. 5.** The moisture ingress characteristics for all situations. The dashed line separates the trends for varying encapsulants (on the left) and varying backsheets (on the right). The choice of encapsulant affects $\tau_{95\%}$, $A$, and $\tau_{0.01}$, whereas the backsheet only significantly affects $\tau_{95\%}$.

The seasonal deviation $A$ is higher with TPO, indicating more significant fluctuations in $RMC$. These fluctuations are driven more by changes in solubility than by changes in concentration. TPO's high activation energy for solubility makes its solubility more sensitive to temperature, leading to pronounced seasonal variations in $RMC$.

The backsheet material predominantly impacts the moisture saturation time. TPSiOx, with a lower pre-exponential factor, exhibits a longer $\tau_{95\%}$ and $\tau_{0.01}$. However, the encapsulant's influence is more significant overall, as moisture travels a longer path through it than through the backsheet.

### 4.2. Effect of climate

Next, we vary the climate and examine its effect on the moisture ingress. In all simulations, EVA was used as the encapsulant and PET as the backsheet. Fig. 6 presents the simulated moisture ingress for these locations. As with the materials, Fig. 7 provides a detailed comparison of the characteristics for each climate.

$RMC_{eq}$ is highest in continental locations, driven by their high effective relative humidity. Despite outdoor conditions not being constant, the average $RH_{eff}$ serves as a good indicator of $RMC_{eq}$. Moisture ingress occurs fastest in tropical climates, evidenced by the smallest $\tau_{95\%}$ and $\tau_{0.01}$ values. This is due to the higher module temperatures in these regions, which increase the diffusion coefficient and accelerate moisture ingress.

Finally, the seasonal deviation is most pronounced in continental climates, which have the largest seasonal temperature variations. These fluctuations cause significant changes in solubility over the seasons, leading to varying $RMC$.

Comparing the effect of material and climate, it can be seen that climate choice produces a wider range of $RMC_{eq}$ and $A$ values than material variation just in Freiburg. If PDMS is excluded then this also holds for saturation and ingress times. This indicates that it might be reasonable to adjust the PV module design to the climates rather than trying to find a one fits all global solution as the PV industry grows in the future.

## 5. Analytical model

In the previous section, we identified clear trends between the moisture ingress characteristics and the operating conditions of PV modules. This opens up the possibility of predicting these characteristics and modeling the moisture ingress without relying on computationally intensive simulations. This section introduces an analytical model that uses empirically determined parameters for simulating moisture ingress.

### 5.1. Analytical equation

From our observations, the yearly average $RMC$ starts at zero and gradually approaches an equilibrium value, $RMC_{eq}$, over time. This relationship can be expressed as

$$RMC(t) = RMC_{eq}\left(1 - e^{-\frac{t}{\tau_{95\%}}\ln(20)}\right), \tag{8}$$

where the term $\ln(20)$ is included to ensure that $RMC(t) = 0.95 \cdot RMC_{eq}$ at $t = \tau_{95\%}$.

Additionally, there is a seasonal trend in moisture ingress, which can be described using a sinusoidal function with an amplitude of $\frac{A}{2}$. By incorporating this seasonal variation, the equation extends to

$$RMC(t) = \left(RMC_{eq} + \frac{A}{2} \cdot \cos\left(2\pi(t-\phi)\right)\right) \cdot \left(1 - e^{-\frac{t}{\tau_{95\%}}\ln(20)}\right), \tag{9}$$

where $\phi$ represents the phase shift and is equal to the coldest moment of the year, as $RMC$ tends to peak on colder days. It should be noted that both $t$ and $\phi$ are expressed in years.

Upon closer inspection, we notice that moisture ingress deviates from this pattern in the initial years. Due to the time required for water to permeate through the backsheet and encapsulant, there is a delay before RMC reaches significant values. This delay, characterized by $\tau_{0.01}$, can be incorporated into the equation by applying a time shift in the exponential term. Thus, the final form of our analytical equation is:

$$RMC(t) = \left(RMC_{eq} + \frac{A}{2} \cdot \cos\left(2\pi(t-\phi)\right)\right) \cdot \left(1 - e^{-\frac{t-\tau_{0.01}}{\tau_{95\%}}\ln(20)}\right). \tag{10}$$

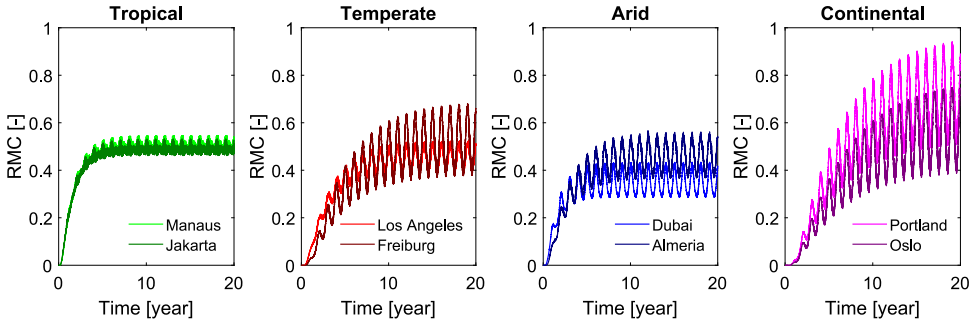


**Fig. 6.** The moisture ingress of a PV module with an EVA encapsulant and PET backsheet for different locations. The locations represent four different climates.

**Table 3**
The coefficients for the moisture ingress characteristics for all materials.

| | $RMC_{eq}$ | | $\tau_{95\%}$ | | $A$ | | $\tau_{0.01\%}$ | |
|---|---|---|---|---|---|---|---|---|
| | $c_{1,RMC}$ [-] | $c_{2,RMC}$ [-] | $c_{1,\tau95\%}$ [y/K] | $c_{2,\tau95\%}$ [y] | $c_{1,A}$ [-] | $c_{2,A}$ [-] | $c_{1,\tau0.01}$ [y/K] | $c_{2,\tau0.01}$ [y] |
| EVA | 1.23 | −0.170 | −0.456 | 144 | 0.0140 | −0.0303 | −0.0455 | 14.1 |
| TPO | 1.28 | −0.149 | −0.509 | 161 | 0.0221 | −0.0474 | −0.0543 | 16.8 |
| PDMS | 1.16 | −0.158 | −0.110 | 35.2 | 0.00818 | 0.0317 | −0.00176 | 0.575 |
| PET | 1.23 | −0.170 | −0.456 | 144 | 0.0140 | −0.0303 | −0.0455 | 14.1 |
| TPT | 1.28 | −0.187 | −0.383 | 121 | 0.0145 | −0.0336 | −0.0423 | 13.0 |
| $TPSiO_x$ | 0.892 | −0.0170 | −0.501 | 160 | 0.0116 | −0.00759 | −0.0541 | 16.9 |
| PA | 1.17 | −0.160 | −0.495 | 156 | 0.0134 | −0.0293 | −0.0484 | 15.0 |

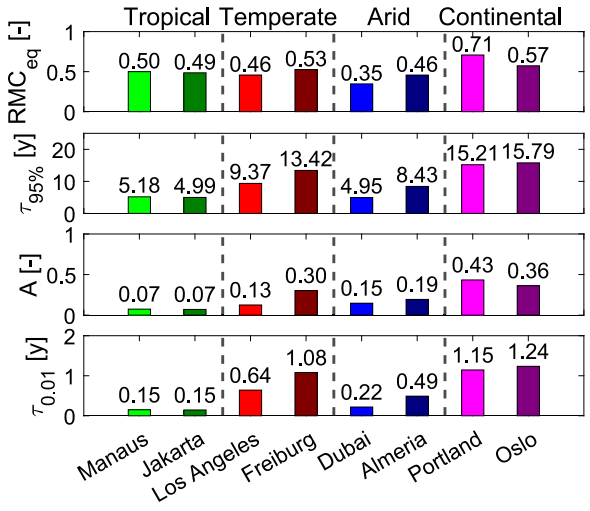


**Fig. 7.** The characteristics for the different locations. It can be seen that the moisture enters faster for tropical locations (lower $\tau_{95\%}$ and $\tau_{0.01}$), but reaches a higher equilibrium for continental climates.

### 5.2. Characteristic trends

To utilize this analytical model as a substitute for the FEM model, we need to determine the specific characteristics of the PV module for a given location. From the previous section, we know that $RMC_{eq}$ and $A$ are related to the effective RH and $\Delta T_{mod}$, respectively. Meanwhile, $\tau_{95\%}$ and $\tau_{0.01}$ are linked to $T_{mod}$.

Fig. 8 demonstrates the relationship between these characteristics and their corresponding stress factors for a PV module with EVA encapsulant and PET backsheet. Each characteristic can be approximated by a linear fit in the form $y = c_1 \cdot x + c_2$. As discussed, these characteristics are influenced not only by location but also by the materials used. Therefore, the coefficients $c_1$ and $c_2$ differ for each material, as shown in Table 3. These coefficients enable us to predict the moisture ingress characteristics under various operating conditions.

### 5.3. Analytical model development

Using the coefficients provided in Table 3, we can predict the necessary characteristics for our analytical model in Eq. (10) and reconstruct the moisture ingress under specific conditions.

Fig. 9 illustrates the reconstructed moisture ingress for a PV module with EVA encapsulant and PET backsheet in Freiburg. The predicted characteristics, derived from the corresponding coefficients and stress factors (shown in Table 2), align closely with the simulated results. To quantify this accuracy, we define the reconstruction error ($\epsilon$) of the reconstruction as

$$\epsilon = \frac{\int_0^{N_{years}} |RMC_{sim}(t) - RMC_{rec}(t)| dt}{N_{years}}, \tag{11}$$

where $N_{years}$ is the simulated lifetime, and $RMC_{sim}(t)$ and $RMC_{rec}(t)$ are the simulated and reconstructed $RMC$, respectively. The value of $\epsilon$ represents the average deviation between the reconstructed and simulated $RMC$.

We applied this reconstruction method to various materials and locations. Fig. 10 displays the average deviation for all materials. Across all cases, the average $\epsilon$ remains below 0.05, indicating that the moisture ingress can be accurately reconstructed with a deviation of less than 0.05. This demonstrates that our empirical model can effectively predict moisture ingress in new locations without resorting to computationally intensive FEM simulations.

Besides having a low average deviation $\epsilon$ for the tested cases, the analytical model introduced in form of Eq. (10) is also more simple than the analytical models found in literature [38] or two dimensions [15]. As, these literature models rely on lengthy equations involving infinite summations, making their implementation more complex. Furthermore, they use fixed values for diffusivity and solubility, while our model accounts for their temperature dependence. In addition the literature models calculate concentration rather than RMC, which our results indicate to be the more useful measure. This highlights some clear advantages of our analytical model over those commonly used in the literature.

## 6. Impact on degradation

Lastly, we examine how the degradation profile of PV modules due to moisture ingress changes when replacing $RH_{eff}$ with $RMC$ as the stress factor. We use the Peck model [4,5,39] to calculate the moisture-induced degradation rate, written as

$$k(t) = K_0 \cdot e^{-\frac{E_{a,deg}}{k_b \cdot T_{mod}(t)}} \cdot X(t)^n, \tag{12}$$

where $k(t)$ is the degradation rate at time $t$, $K_0$ is the degradation pre-exponential constant, $E_{a,deg}$ is the degradation activation energy, $k_b$ is the Boltzmann constant, $n$ is a model parameter, and $X$ is either $RH_{eff}$ or $RMC$.

To determine the parameters in Eq. (12) we fit the equation to the damp-heat experiments performed by Zhu [40]. The used values for $A$, $E_{a,deg}$, and $n$ are $8 \cdot 10^7$ %/h, 0.809 eV, and 1.5 respectively. It should be realized that this fitting is performed for PV modules with EVA encapsulant and PET backsheet.

The calculated degradation rate can be used to determine the normalized power of the PV module ($P_{norm}$) throughout its lifetime. This is calculated by iterating

$$P_{norm}(t + \Delta t) = P_{norm}(t) \cdot (1 - k(t) \cdot \Delta t), \tag{13}$$

where $\Delta t$ is the time step, which is set at 24 h in this study. It is important to note that $k(t)$ only accounts for degradation caused by moisture ingress, excluding other degradation mechanisms. However,

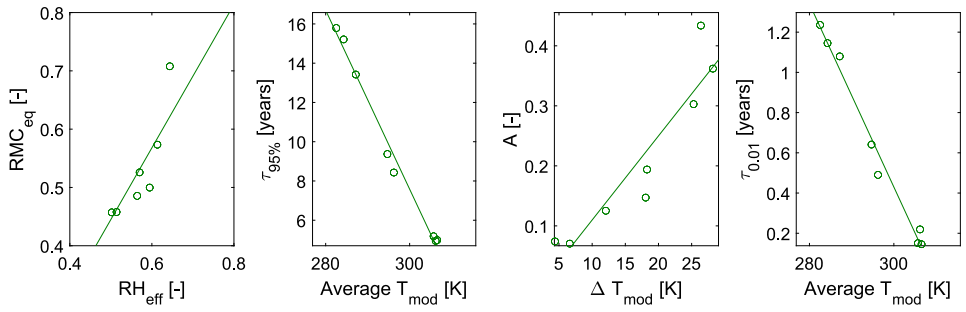


**Fig. 8.** The relation between the different characteristics and the stress factors. For each characteristic, a linear trend can be made with respect to the corresponding stress factor. Only the trend lines for the reference PV module (EVA as encapsulant and PET as backsheet) is shown.

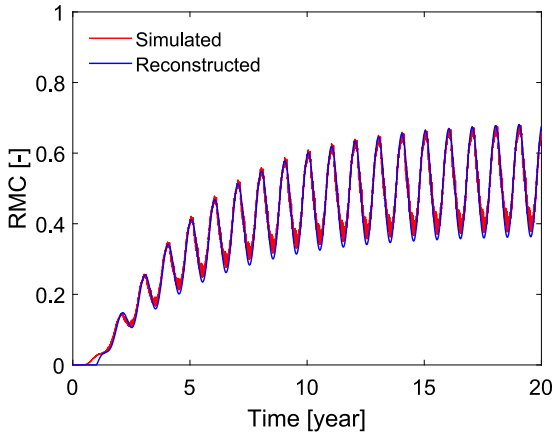


**Fig. 9.** The comparison between the reconstructed and simulated moisture ingress for the reference PV module in Freiburg. It can be seen that the reconstruction closely matches the simulation.

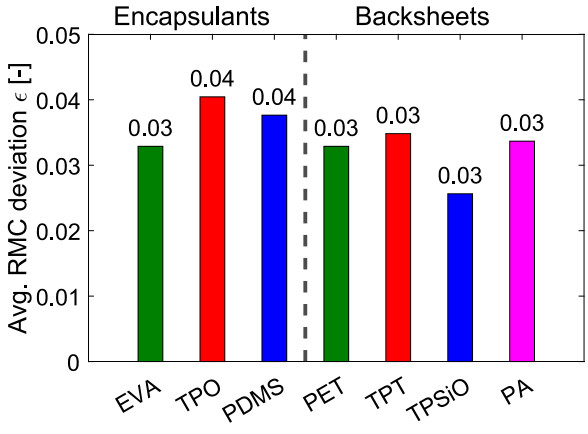


**Fig. 10.** The average RMC deviation between FEM simulation and analytical model for the different materials. For each material, this is applied for all locations and the average deviation is shown.

this approach allows us to directly compare the impact of using $RH_{eff}$ versus $RMC$ as the stress factor.

Fig. 11 illustrates $P_{norm}$ across various climates. The dashed lines represent $P_{norm}$ calculated using $RH_{eff}$, while the solid lines use $RMC$. Using $RH_{eff}$ as the stress factor results in a consistent annual degradation rate, causing a linear decline in normalized power over time. Conversely, when $RMC$ is used as the stress factor, the normalized power remains relatively stable in the initial years because the moisture has not yet penetrated the module fully. As moisture ingress progresses, the degradation rate accelerates, leading to a faster decline in normalized power. This aligns with literature, which indicates that degradation mechanisms associated with moisture ingress tend to increase over time [41].

This comparison demonstrates that using $RMC$ as the stress factor could potentially be more accurate for the prediction of physical degradation in PV modules. Further work including additional validation is needed to fully compare the two stress factors.

## 7. Conclusion

In this study, we developed and validated a model to simulate and analyze moisture ingress in PV modules. Using COMSOL Multiphysics, a FEM model is built, which incorporated Fickian diffusion and Henry's law. We validated the model with indoor experiments and outdoor simulations from literature.

Our simulations revealed critical insights into the effects of material selection and climate conditions on moisture ingress. By comparing different encapsulant and backsheet materials, we identified that the choice of material significantly impacts the rate at which moisture enters the module, but also the seasonal fluctuations. Specifically, materials like PDMS and TPO show faster moisture ingress and higher fluctuations in $RMC$ due to their diffusion and solubility characteristics. The backsheet material, while influential, has a smaller effect on the RMC at the front compared to the encapsulant, primarily due to the longer diffusion path through the encapsulant.

Further, we examined the impact of varying climatic conditions on moisture ingress using eight geographically diverse locations. The results showed that moisture ingress and its effects are highly sensitive to climate, with tropical climates experiencing the fastest moisture penetration due to higher ambient temperatures. In contrast, continental climates showed the highest equilibrium moisture content due to high $RH_{eff}$ in these locations. Overall, the impact of the climate has a larger impact on the moisture ingress than the choice of material, implying that the PV module design should be adjusted for different climates.

To simplify the prediction of moisture ingress without relying on complex and time-consuming simulations, we developed an analytical model. This model uses empirical relationships between the characteristics and the stress factors. We show that we can reconstruct the moisture ingress results with a deviation lower than 0.05 for all conditions.

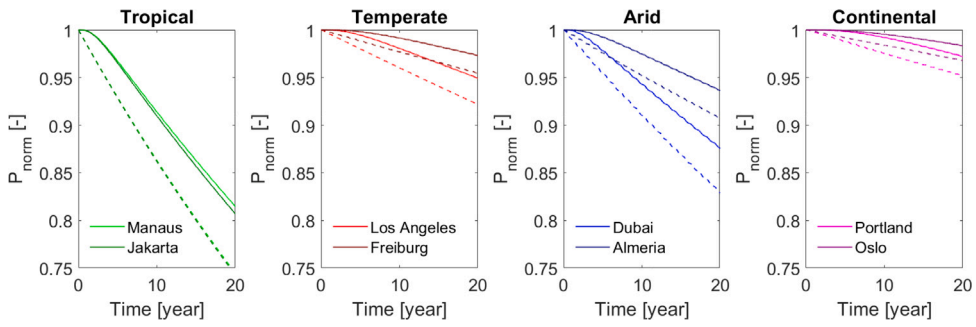


**Fig. 11.** The effect of the degradation profile due to the replacement of $RH_{eff}$ with $RMC$. The dashed line indicates the degradation trend calculated with RH, and the solid line represents the degradation trend calculated with $RMC$.

We also explored the implications of using $RMC$ instead of $RH_{eff}$ as the stress factor in degradation models. The Peck model is used to calculate the normalized power through the module's lifetime.

Our findings show that using $RMC$ as stress factor leads to the degradation rate increasing with time, which is more consistent with literature. This suggests that degradation models can improve the physical accuracy by including $RMC$ as stress factor.

## CRediT authorship contribution statement

**Youri Blom:** Writing – original draft, Visualization, Validation, Software, Methodology. **Daniel Jimenez Pelarda:** Validation, Methodology. **Tabitha Minett:** Writing – review & editing, Software, Methodology. **Ismail Kaaya:** Writing – review & editing, Methodology. **Nikoleta Kyranaki:** Writing – review & editing, Methodology. **Rudi Santbergen:** Writing – review & editing, Supervision. **Olindo Isabella:** Writing – review & editing, Supervision. **Malte Ruben Vogt:** Writing – review & editing, Supervision, Methodology.

## Declaration of Generative AI and AI-assisted technologies in the writing process

During the preparation of this work the author(s) used ChatGPT in order to paraphrase sentences and improve the language and readability. After using this tool/service, the author(s) reviewed and edited the content as needed and take(s) full responsibility for the content of the publication

## Declaration of competing interest

The authors declare that they have no known competing financial interests or personal relationships that could have appeared to influence the work reported in this paper.

## Appendix A. Exact geometry of basic model

The main text has introduced both the basic and the advanced model. As the basic model has a rather complex geometry, the exact values for the different dimensions are shown in Fig. A.1, allowing the model to be easily recreated.

## Appendix B. Implementation of advanced model

The exact dimensions in the advanced model are shown in Fig. B.1. As mentioned in the main text, the encapsulant is divided into bulk and channel regions. The channel is composed of 15 by 32 units, where each unit has a length and width of 62.5 μm. It should be noted that the width of the horizontal and vertical channels ($W_H$ and $W_V$) used in the model are slightly larger than the width of the diagonal channels ($W_D$). Other than having different values for the diffusion coefficient, the bulk and channel regions are considered to be identical in the COMSOL simulation.

## Appendix C. Calculation seasonal change module temperature

In Section 4, $\Delta T_{mod}$ is introduced as stress factor. This stress factor represents the seasonal fluctuations throughout the operating lifetime. It is calculated by defining $T_{upper}$ and $T_{lower}$, which represent, respectively, the maximum and minimum temperature in a certain time window (see Fig. C.1). $\Delta T_{mod}$ is then calculated as

$$\Delta T_{mod} = \frac{\left(\max(T_{upper}) - \min(T_{upper})\right) + \left(\max(T_{lower}) - \min(T_{lower})\right)}{2}. \quad \text{(C.1)}$$

## Data availability

We have included the data from all simulations from COMSOL as supporting information. Any other data is available upon request.

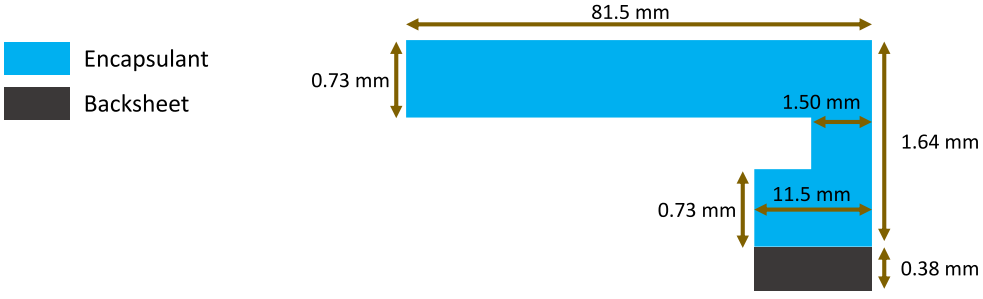


**Fig. A.1.** The exact value of the dimensions used in the basic model. Please note that the drawing is not too scale.

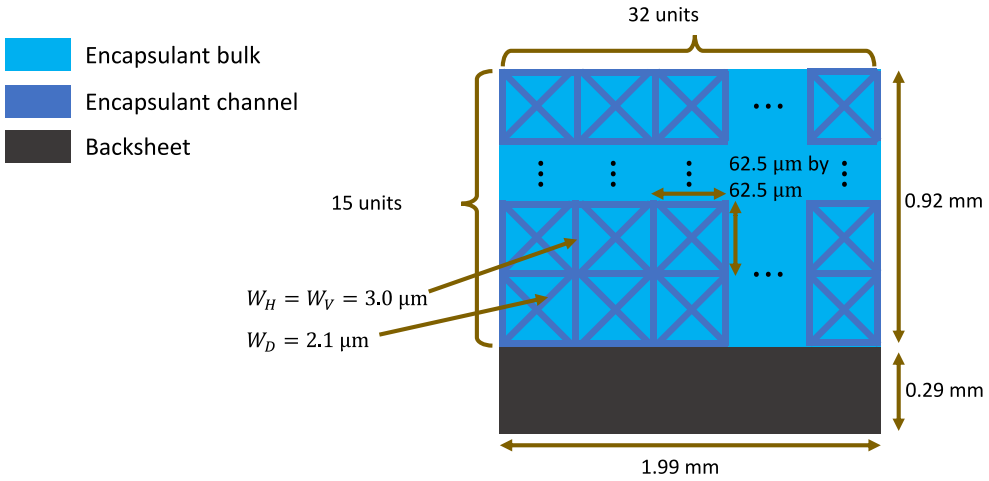


**Fig. B.1.** The exact value of the dimensions used in the advanced model. Please note that the drawning is not too scale.

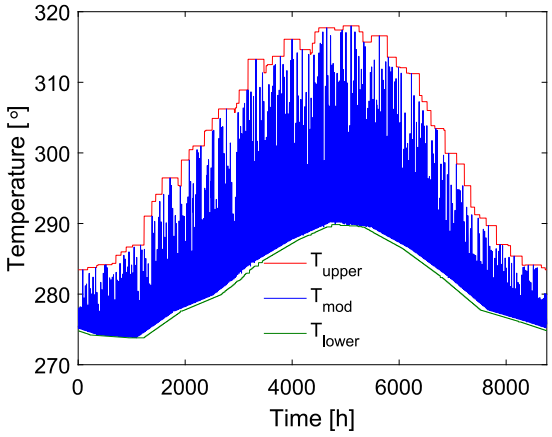


**Fig. C.1.** The calculation of the $\Delta T_{mod}$. Based on $T_{mod}$, $T_{upper}$ and $T_{lower}$ are determined, which are used for $\Delta T_{mod}$. As example the temperature profile of Freiburg is selected.

## References


[1] IRENA, Renewable Power Generation Costs in 2022, Tech. Rep., IRENA, 2023.

[2] M. Köntges, S. Kurtz, C. Packard, U. Jahn, K.A. Berger, K. Kato, T. Friesen, H. Liu, M. Van Iseghem, Review of Failures of Photovoltaic Modules, Tech. Rep., International Energy Agency, 2014.

[3] M. Aghaei, A. Fairbrother, A. Gok, S. Ahmad, S. Kazim, K. Lobato, G. Oreski, A. Reinders, J. Schmitz, M. Theelen, P. Yilmaz, J. Kettle, Review of degradation and failure phenomena in photovoltaic modules, Renew. Sustain. Energy Rev. 159 (2022) 112160, http://dx.doi.org/10.1016/j.rser.2022.112160, URL https://www.sciencedirect.com/science/article/pii/S1364032122000880.

[4] I. Kaaya, M. Koehl, A.P. Mehilli, S. de Cardona Mariano, K.A. Weiss, Modeling Outdoor Service Lifetime Prediction of PV Modules: Effects of Combined Climatic Stressors on PV Module Power Degradation, IEEE J. Photovoltaics 9 (4) (2019) 1105–1112, http://dx.doi.org/10.1109/JPHOTOV.2019.2916197.

[5] A. Bala Subramaniyan, R. Pan, J. Kuitche, G. TamizhMani, Quantification of Environmental Effects on PV Module Degradation: A Physics-Based Data-Driven Modeling Method, IEEE J. Photovoltaics 8 (5) (2018) 1289–1296, http://dx.doi.org/10.1109/JPHOTOV.2018.2850527.

[6] A.A.Q. Hasan, A. Ahmed Alkahtani, S.A. Shahahmadi, M. Nur E. Alam, M.A. Islam, N. Amin, Delamination-and Electromigration-Related Failures in Solar Panels—A Review, Sustainability 13 (12) (2021) 6882, http://dx.doi.org/10.3390/su13126882.

[7] O.K. Segbefia, A.G. Imenes, T.O. Sætre, Moisture ingress in photovoltaic modules: A review, Sol. Energy 224 (2021) 889–906, http://dx.doi.org/10.1016/j.solener.2021.06.055, URL https://www.sciencedirect.com/science/article/pii/S0038092X21005375.

[8] O.K. Segbefia, N. Akhtar, T.O. Sætre, Moisture induced degradation in field-aged multicrystalline silicon photovoltaic modules, Sol. Energy Mater. Sol. Cells 258 (2023) 112407, http://dx.doi.org/10.1016/j.solmat.2023.112407.

[9] M. Koehl, M. Heck, S. Wiesmeier, Modelling of conditions for accelerated lifetime testing of humidity impact on PV-modules based on monitoring of climatic data, Sol. Energy Mater. Sol. Cells 99 (2012) 282–291, http://dx.doi.org/10.1016/j.solmat.2011.12.011, URL https://www.sciencedirect.com/science/article/pii/S0927024811006921, 9th International Meeting on Electrochromism.

[10] M.D. Kempe, Modeling of rates of moisture ingress into photovoltaic modules, Sol. Energy Mater. Sol. Cells 90 (16) (2006) 2720–2738, http://dx.doi.org/10.1016/j.solmat.2006.04.002.

[11] P. Hülsmann, K.-A. Weiss, Simulation of water ingress into PV-modules: IEC-testing versus outdoor exposure, Sol. Energy 115 (2015) 347–353, http://dx.doi.org/10.1016/j.solener.2015.03.007.

[12] S. Mitterhofer, J. Ascencio-Vásquez, X. Gu, Worldwide moisture ingress evaluation in photovoltaic modules using finite element simulations and machine learning, in: WCPEC, 2022.

[13] S. Mitterhofer, J. Slapšak, A. Astigarraga, D. Moser, G.O. Hernandez, P.V. Chiantore, W. Luo, Y.S. Khoo, J. Rabanal-Arabach, E. Fuentealba, P. Ferrada, M. Trigo Gonzalez, J. Ascencio-Vásquez, M. Topič, M. Jankovec, Measurement and Simulation of Moisture Ingress in PV Modules in Various Climates, IEEE J. Photovoltaics 14 (1) (2024) 140–148, http://dx.doi.org/10.1109/JPHOTOV.2023.3323808.

[14] D.J. Coyle, Life prediction for CIGS solar modules part 1: modeling moisture ingress and degradation, Prog. Photovolt., Res. Appl. 21 (2) (2013) 156–172, http://dx.doi.org/10.1002/pip.1172.

[15] S. Marwaha, K. Ghosh, Analytical Modeling of Diffusion of Moisture in Silicon Photovoltaic Module under Damp Heat Testing Condition, Silicon 14 (9) (2022) 4757–4766, http://dx.doi.org/10.1007/s12633-021-01156-7.

[16] COMSOL, Inc, COMSOL Multiphysics Reference Manual, version 6.2, URL www.comsol.com.

[17] S. Mitterhofer, C. Barretta, L.F. Castillon, G. Oreski, M. Topič, M. Jankovec, A dual-transport model of moisture diffusion in PV encapsulants for finite-element simulations, IEEE J. Photovoltaics 10 (1) (2020) 94–102, http://dx.doi.org/10.1109/JPHOTOV.2019.2955182.

[18] N. Kyranaki, A. Smith, K. Yendall, D.A. Hutt, D.C. Whalley, R. Gottschalg, T.R. Betts, Damp-heat induced degradation in photovoltaic modules manufactured with passivated emitter and rear contact solar cells, Prog. Photovolt., Res. Appl. 30 (9) (2022) 1061–1071, http://dx.doi.org/10.1002/pip.3556.

[19] L.M. Shaker, A. Alamiery, W.N.R.W. Isahak, W.K. Al-Azzawi, Corrosion in solar cells: challenges and solutions for enhanced performance and durability, J. Opt. (2023) http://dx.doi.org/10.1007/s12596-023-01277-9.

[20] Adolph Fick, V. On liquid diffusion, Lond. Edinb. Dublin Philos. Mag. J. Sci. 10 (63) (1855) 30–39, http://dx.doi.org/10.1080/14786445508641925.

[21] N. Kim, C. Han, Experimental characterization and simulation of water vapor diffusion through various encapsulants used in PV modules, Sol. Energy Mater. Sol. Cells 116 (2013) 68–75, http://dx.doi.org/10.1016/j.solmat.2013.04.007, URL https://www.sciencedirect.com/science/article/pii/S0927024813001724.

[22] D. Faiman, Assessing the outdoor operating temperature of photovoltaic modules, Prog. Photovolt., Res. Appl. 16 (4) (2008) 307–315, http://dx.doi.org/10.1002/pip.813.

[23] W. Henry, J. Banks, III. Experiments on the quantity of gases absorbed by water, at different temperatures, and under different pressures, Philos. Trans. R. Soc. Lond. 93 (1803) 29–274, http://dx.doi.org/10.1098/rstl.1803.0004.

[24] N. Kyranaki, Corrosion in Crystalline Silicon Photovoltaic Modules and the Influence on Performance (Ph.D. thesis), Loughborough University, 2021.

[25] D.R. Stull, Vapor pressure of pure substances. Organic and inorganic compounds, Ind. Eng. Chem. 39 (1947) 517–540.

[26] M. Gagliardi, P. Lenarda, M. Paggi, A reaction-diffusion formulation to simulate EVA polymer degradation in environmental and accelerated ageing conditions, Sol. Energy Mater. Sol. Cells 164 (2017) 93–106, http://dx.doi.org/10.1016/j.solmat.2017.02.014.

[27] V. Naumann, K. Ilse, M. Pander, J. Tröndle, K. Sporleder, C. Hagendorf, Influence of soiling and moisture ingress on long term PID susceptibility of photovoltaic modules, AIP Conf. Proc. 2147 (1) (2019) 090005, http://dx.doi.org/10.1063/1.5123873.

[28] D. Sonntag, Important new values of the physical constants of 1986, vapor pressure formulations based on ITS-90 and psychrometer formulae, Z. Für Meteorol. 1990 (63) (1990) 340–344.

[29] E.R. Anagha, S.V. Kulkarni, N. Shiradkar, Moisture ingress modeling in c-Si PV modules using finite element simulations based on dual transport diffusion, in: 2021 IEEE 48th Photovoltaic Specialists Conference, PVSC, 2021, pp. 2470–2474, http://dx.doi.org/10.1109/PVSC43889.2021.9518770.

[30] W. Lei, M.K. Rigozzi, D.R. McKenzie, The physics of confined flow and its application to water leaks, water permeation and water nanoflows: a review, Rep. Progr. Phys. 79 (2) (2016) 025901, http://dx.doi.org/10.1088/0034-4885/79/2/025901.

[31] B. Bhattacharyya, W. Huffman, W. Jahsman, B. Natarajan, Moisture absorption and mechanical performance of surface mountable plastic packages, in: 38th Electronics Components Conference 1988., Proceedings, 1988, pp. 49–58, http://dx.doi.org/10.1109/ECC.1988.12569.

[32] E. Wong, R. Rajoo, Moisture absorption and diffusion characterisation of packaging materials—-advanced treatment, Microelectron. Reliab. 43 (12) (2003) 2087–2096, http://dx.doi.org/10.1016/S0026-2714(03)00378-0, URL https://www.sciencedirect.com/science/article/pii/S0026271403003780.

[33] J.E. Gonçalves, T. van Hooff, D. Saelens, Simulating building integrated photovoltaic facades: Comparison to experimental data and evaluation of modelling complexity, Appl. Energy 281 (2021) 116032, http://dx.doi.org/10.1016/j.apenergy.2020.116032, URL https://www.sciencedirect.com/science/article/pii/S0306261920314707.

[34] M.D. Kempe, A.A. Dameron, M.O. Reese, Evaluation of moisture ingress from the perimeter of photovoltaic modules, Prog. Photovolt., Res. Appl. 22 (11) (2014) 1159–1171, http://dx.doi.org/10.1002/pip.2374, URL https://onlinelibrary.wiley.com/doi/abs/10.1002/pip.2374.

[35] P. Hülsmann, K.-A. Weiß, M. Köhl, Temperature-dependent water vapour and oxygen permeation through different polymeric materials used in photovoltaic-modules, Prog. Photovolt., Res. Appl. 22 (4) (2014) 415–421, http://dx.doi.org/10.1002/pip.2273, URL https://onlinelibrary.wiley.com/doi/abs/10.1002/pip.2273.

[36] M. Kottek, J. Grieser, C. Beck, B. Rudolf, F. Rubel, World Map of the Köppen-Geiger climate classification updated, Meteorol. Zeitschrif 15 (3) (2006) 259–263.

[37] J. Remund, S. Müller, M. Schmutz, P. Graf, Meteonorm version 8, 2020, METEOTEST (www.meteotest.com).

[38] M. Kempe, Control of moisture ingress into photovoltaic modules, in: Conference Record of the Thirty-First IEEE Photovoltaic Specialists Conference, 2005, 2005, pp. 503–506, http://dx.doi.org/10.1109/PVSC.2005.1488180.

[39] S. Lindig, I. Kaaya, K.-A. Weiss, D. Moser, M. Topic, Review of statistical and analytical degradation models for photovoltaic modules and systems as well as related improvements, IEEE J. Photovoltaics 8 (6) (2018) 1773–1786, http://dx.doi.org/10.1109/JPHOTOV.2018.2870532.

[40] J. Zhu, M. Koehl, S. Hoffmann, K.A. Berger, S. Zamini, I. Bennett, E. Gerritsen, P. Malbranche, P. Pugliatti, A. Di Stefano, F. Aleo, D. Bertani, F. Paletta, F. Roca, G. Graditi, M. Pellegrino, O. Zubillaga, F.J.C. Iranzo, A. Pozza, T. Sample, R. Gottschalg, Changes of solar cell parameters during damp-heat exposure, Prog. Photovolt., Res. Appl. 24 (10) (2016) 1346–1358, http://dx.doi.org/10.1002/pip.2793, URL https://onlinelibrary.wiley.com/doi/abs/10.1002/pip.2793.

[41] D.C. Jordan, T.J. Silverman, B. Sekulic, S.R. Kurtz, PV degradation curves: non-linearities and failure modes, Prog. Photovolt., Res. Appl. 25 (7) (2017) 583–591, http://dx.doi.org/10.1002/pip.2835, URL https://onlinelibrary.wiley.com/doi/abs/10.1002/pip.2835.